Journal of Power Sources 186 (2009) 229–237

Contents lists available at ScienceDirect

Journal of Power Sources

journal homepage: www.elsevier.com/locate/jpowsour

A composite anode with reactive methanol filter for direct methanol fuel cell

Chieh-Hao Wan [a,*], Chien-Heng Lin [b]

[a] Department of Energy Engineering, MingDao University, Changhua 52342, Taiwan
[b] Institute of Materials Science and Engineering, National Chung Hsing University, Taichung, Taiwan

ARTICLE INFO

Article history:
Received 31 August 2008
Received in revised form 14 October 2008
Accepted 15 October 2008
Available online 8 November 2008

Keywords:
Methanol crossover
Nanometer-sized catalyst particles
Filtering effect
Impregnation–reduction method
Composite anodes

ABSTRACT

Two composite electrode structures for direct methanol fuel cells comprising an outer, middle and an inner catalyst layers, are proposed to suppress methanol crossover and improve the utilization efficiency of methanol fuel. These two composite anodes have structures I and II, and are prepared by a combination of screen-printing, direct-printing and impregnation–reduction (IR) methods. The inner layer of these two composite anodes, which are prepared by IR method, is a layer of nanometer-sized Pt_{37}–Ru_{63}/Pt or Pt_{37}–Ru_{63}/Pt_{20}–Ru_{80} catalyst particles deposited in the PEM anode side serving as the reactive methanol filter layer. The suppression of methanol crossover and the membrane electrode assembly (MEA) performance of the proposed structures are compared to those of the normal-MEA structure with PEM without IR treatment. The mechanisms of the suppression of methanol crossover are investigated. Experimental results show that the MEA-I and MEA-II improve the suppression of methanol crossover by up to 22% and 33% compared to the normal-MEA structure, respectively, and yield a 12% and 18% better MEA performance than the normal-MEA structure, respectively. The filtering and electrode effects of a layer of nanometer-sized Pt_{37}–Ru_{63}/Pt or Pt_{37}–Ru_{63}/Pt_{20}–Ru_{80} catalyst particles deposited in the PEM anode side contribute to the suppression of methanol crossover and performance enhancement.

1. Introduction

Direct methanol fuel cell (DMFC) is a promising energy conversion device especially attractive for portable application. The major advantages of a DMFC over PEMFCs—an on-board methanol reformer, include (1) a simplified system, (2) reduced start-up time, (3) ease of maintenance, etc. However, two issues must be addressed to increase the efficiency of DMFCs before this technology is commercially viable. The first issue concerns the development of high-activity anode catalyst with a suitable anode structure for direct methanol oxidation [1–6]. The second issue concerns the prevention of methanol crossover from anode to cathode through the proton exchange membrane (PEM). Methanol crossover markedly reduces both the cathode potential and fuel utilization due to chemical short-circuit reaction between the crossed-over methanol and O_2 at the cathode.

Ren et al. [7] investigated the level of methanol crossover in Nafion® membranes while optimizing operating conditions and improving performance. Efforts to develop new PEMs with reduced crossover effect have also been reported [8–11]. Wainright et al. [8,9] developed a new acid-doped polybenzimidazole PEM to suppress methanol crossover. The results revealed that the suppression of methanol crossover by this new PEM exceeded that of the Nafion membrane by one order of magnitude with the same performance. This new PEM can conduct protons at 130–150 °C, and can thereby use vapor methanol as the anode fuel. Methanol crossover can be efficiently reduced by incorporating a suitable amount of Ce^{4+} ions into the PEM [12]. Metal hybrid materials, such as Pd, have been coated onto the surface of Nafion® membrane as barriers to methanol [13]. This sandwich structure offers superior suppression of methanol crossover, but substantially reduces the membrane electrode assembly (MEA) performance, unfortunately.

In the past, the impregnation–reduction (IR) method was often employed to fabricate water electrolysis electrodes [14–16]. Fujiwara et al. [17] were the first to use the IR method to prepare a MEA for the DMFC. They found that the advantages of the IR method in preparing a catalyst layer include easier control of the alloy composition, the loadings, the layer thickness and the adhesion of the Pt–Ru alloy catalyst onto the PEM. The obtained catalyst layer has a porous microstructure, which facilitates the release of the evolved CO_2. The IR method reduces the risk of electrodes' peeling from the PEM because of the swelling of the PEM on the absorbing methanol. Its use is attractive for applications of various solid polymer electrolyte materials with low heat-resistance and various shapes, and the resulting catalytic layer is embedded at 3–4 μm from the membrane surface to produce a porous and hydrophilic layer.

* Corresponding author. Tel.: +886 4 8876660x8510; fax: +886 4 8890445.
E-mail addresses: chiehhao@mdu.edu.tw, n3883115@xuite.net (C.-H. Wan).

0378-7753/$ – see front matter © 2008 Elsevier B.V. All rights reserved.
doi:10.1016/j.jpowsour.2008.10.116

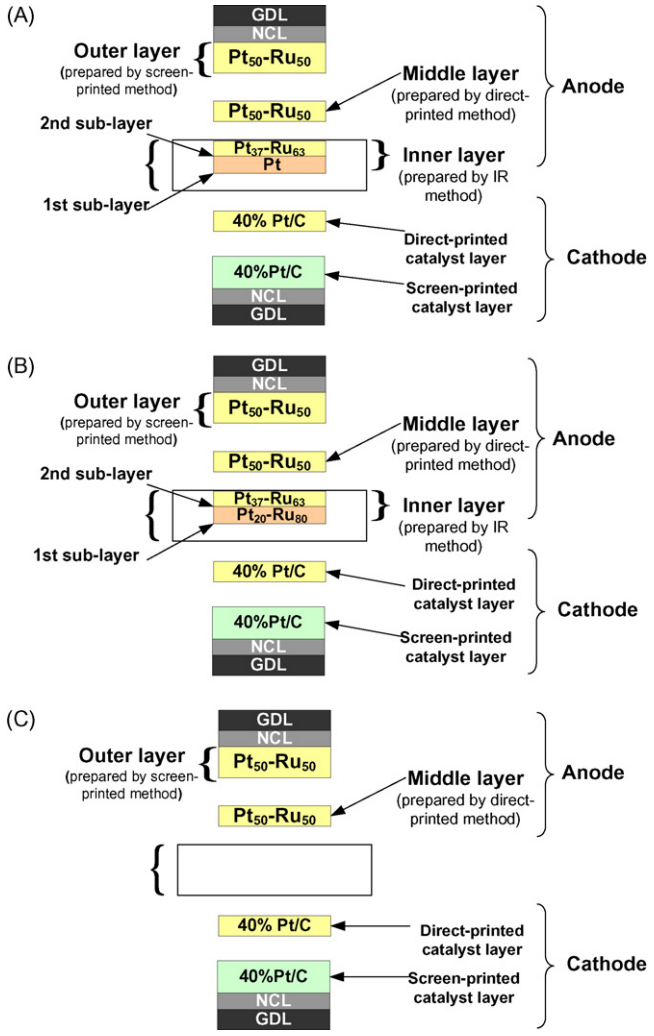

Fig. 1. Diagrams of proposed PEM structures and MEAs: (A) PEM-I and MEA-I; (B) PEM-II and MEA-II; (C) normal-PEM and normal-MEA. ("NCL" and "GDL" stand for "Nafion-carbon layer" and "gas diffusion layer", respectively.)

Chemical reduction is a typical approach for preparing nanometer-sized metal particles in solution. The IR method has shown great potential in the preparation of nanometer-sized Pt particles or a Pt layer in the PEM [18]. Uchida et al. [18] described using new PEMs with highly dispersed nanometer-sized Pt particles to suppress methanol crossover in the DMFC. They found that the effective recombination of the crossed-over methanol and oxygen at the catalytic platinum sites has reduced the amount of methanol that reached the cathode.

A layer of nanometer-sized Pt_{37}–Ru_{63}/Pt or Pt_{37}–Ru_{63}/Pt_{20}–Ru_{80} catalyst particles deposited on the PEM anode side as a "filter" of methanol was prepared by the IR method in this study. Fig. 1 presents the proposed composite anode and MEAs structures. The actual oxidation of methanol that generates electrons and protons occurs primarily at the catalyst layer (Pt_{50}–Ru_{50}/C), formed by the direct-printing method applied on the surface of the PEM and the screen-printing method applied on the gas diffusion layer. In this paper, the effects of a layer of nanometer-sized catalyst particles dispersed in PEM on the suppression of methanol crossover and MEA performance are studied. The mechanism of suppression of methanol crossover and improvement of performance are also analyzed.

2. Experiment

Fig. 1 presents diagrams of the two MEAs that are used herein. The two MEAs differ from each other in the anode composition of the PEM. As shown in Fig. 1(A), PEM comprises two sub-layers—one Pt_{37}–Ru_{63} (nano-particles) and another Pt. These two sub-layers are prepared by first reducing Pt ion, followed by reducing Pt/Ru ions through IR in a PEM to yield the required three-dimensional reaction zone. The PEM and corresponding MEA are denoted as PEM-I and MEA-I, respectively. Table 1 presents the loadings of the two sub-layers—0.27 mg cm^{-2} of Pt_{37}–Ru_{63} (nano-particles), and 0.25 mg cm^{-2} of Pt in the PEM. The total anode Pt_{50}–Ru_{50} catalyst loading on GDL and PEM was 1.62 mg cm^{-2}. The two sub-layers in the PEM in Fig. 1(B) (PEM-II) are similar to those in PEM-I. The only difference between PEM-I and PEM-II is in the first sub-layer—it is a Pt_{20}–Ru_{80} layer rather than a Pt layer. The corresponding MEA is denoted as MEA-II. The loadings of the two sub-layers of Pt_{37}–Ru_{63} and Pt_{20}–Ru_{80} nano-particles dispersed in PEM are 0.27 and 0.25 mg cm^{-2}, respectively, same as that in PEM-I. The total anode Pt_{50}–Ru_{50} catalyst loading on GDL and PEM was 1.63 mg cm^{-2}. Finally, Fig. 1(C) shows a reference MEA that has no metal layer on the anode side in PEM. The structure and catalyst loadings of both anode and cathode of the MEA are identical to those in MEA-I and MEA-II. The MEA is used as a reference MEA to compare the suppression of methanol crossover and MEA performance with MEA-I and MEA-II. The corresponding MEA is denoted as normal-MEA. Notably, the anode Pt_{50}–Ru_{50} catalyst loadings and the cathode Pt catalyst loadings of all MEAs mentioned above are similar to each other, i.e., around 1.63 and 2.26 mg cm^{-2}, respectively. The cathodes of all the MEAs are prepared by printing the Pt catalyst layer on GDL and PEM.

A 50% wet proof carbon cloth is used as a gas diffusion layer. Pt_{50}–Ru_{50}, supplied by Alfa Aesar, is used as the electrocatalyst in the anode of all MEAs. 40 wt% Pt on Vulcan XC-72 (40% Pt/C) is used as the electrocatalyst in the cathode (E-TEK Division of De Nora, Inc., USA). A 5 wt% Nafion solution, in H^+ form, supplied by DuPont, Inc., USA, is used as the proton conductive agent in the catalyst layer. The carbon powder used as the backing layer is Vulcan XC-72. HPLC-grade solvents are used to prepare the catalyst slurry. The following sections describe the fabrications of the electrodes and the MEAs, the measurements of the polarization curves, and the rate of methanol crossover of various MEAs.

Table 1
Characteristics and loadings of MEAs.

Sample code	Loading of inner layer		Loading of middle layer (mg Pt_{50}–Ru_{50} cm^{-2})	Loading of outer layer (mg Pt_{50}–Ru_{50} cm^{-2})	Total anode loading (mg Pt_{50}–Ru_{50} cm^{-2})	Total cathode loading (mg Pt cm^{-2})
	First sub-layer	Second sub-layer				
MEA-I	0.25 mg Pt cm^{-2}	0.27 mg Pt_{37}–Ru_{63} cm^{-2}	0.40	1.23	1.63	2.26
MEA-II	0.25 mg Pt_{20}–Ru_{80} cm^{-2}	0.27 mg Pt_{37}–Ru_{63} cm^{-2}	0.40	1.23	1.63	2.26
Normal-MEA	–	–	0.41	1.24	1.65	2.26

2.1. Preparation of PEM-I and PEM-II by IR method

A suitable amount of the Pt precursor (tetraammineplatinum(II)chloride, $[Pt(NH_3)_4]Cl_2$) was initially placed into preheated water (56 ml) at 45 °C. 28 ml of methanol was added to the solution after the precursor had completely dissolved. The resulting solution was placed in a reactor (designed in-house) that contained pre-treated PEM on the arm side. The impregnation of the Pt precursor into the PEM was conducted at 55 °C for 1.5 h. The PEM was washed with distillated-water until no residue precursor was detected.

The PEM was treated with 1 M H_2SO_4 at 45 °C for 2–3 h to ion-exchange the metal precursor on the surface of the PEM. It was then washed in deionized-water to eliminate any residual H_2SO_4. The PEM that contained the Pt precursor was reduced by adding a 0.1137 g of $NaBH_4$ at 55 °C for 45 min to yield metal Pt in the PEM. The resulted PEM was treated with 1 M HCl at 80 °C for 2 h. This process replaced the remaining un-reacted Pt precursor with protons and yielded the H^+ form of PEM. The first sub-layer (Pt) in PEM was obtained after the HCl had been fully washed out of the PEM. The obtained loading was approximately 0.25 mg cm^{-2}.

The second sub-layer (Pt_{37}–Ru_{63}) in PEM was prepared by similar procedure that used to prepare the first layer of Pt in PEM, as described above, but with different impregnation process and sulfuric acid treatment. For the impregnation process, the mole ratio of Pt to Ru precursors in the solution was 2:3 instead of pure Pt precursors. The Ru precursor used was chloropentaammineruthenium(III)-chloride, $[RuCl(NH_3)_5]Cl_2$, and yielded an atomic ratio of 37:63 for Pt to Ru in the alloy according to the results of EPMA and EDS. The sulfuric acid treatment with 1 M H_2SO_4 following impregnation was neglected because of the need for dispersed surface Pt and Ru precursors in PEM. Note that, the time to reduce this second sub-layer was less than 30 min to yield a loading of 0.27 mg Pt_{37}–Ru_{63} cm^{-2}. This is because the diffusion resistance and the distance of the ions to the second sub-layer on the surface in PEM are smaller than those of the first sub-layer in PEM. PEM-I was obtained after the second sub-layer was deposited.

PEM-II was produced using a similar procedure to that of PEM-I. However, the composition of the solution in the impregnation process of the first sub-layer of PEM-II is different from that for PEM-I: a solution with a mole ratio of 1:4 for Pt to Ru precursor was used instead of pure Pt precursor. To yield a loading of 0.25 mg Pt_{20}–Ru_{80} cm^{-2}, which equals to that of the first sub-layer in PEM-I, a suitable period of time, dependent on the concentration of the precursors and the amount of reductant agent $NaBH_4$, was needed to reduce the precursors of Pt and Ru.

The loadings of the metal Pt and Pt_{37}–Ru_{63} or Pt_{20}–Ru_{80} and Pt_{37}–Ru_{63} in PEM were measured using the TGA method. The PEM without a metal catalyst was initially heated from 30 to 850 °C at a rate of 10 °C min^{-1} under nitrogen purging. Then the residual weight of the PEM was determined. The PEM with the first sub-layer of Pt metal was treated under the same condition. The weight of the Pt metal in PEM was calculated by subtracting the percentage of the residual weight of the metal-containing PEM from the percentage of the residual weight of the PEM without metal. The resulting weight was then divided by the premeasured surface area of the metal-containing PEM used in the TGA measurement to determine the loading of metal in PEM. The loading of the second sub-layer in PEM was obtained similarly. Table 1 presents a summary of the loadings of catalyst layer on PEM-I and PEM-II as well as the loadings of anode and cathode.

2.2. Preparation of anode

Both sides of the carbon cloth (GDL) were printed using Nafion-carbon ink through screen-printing method and dried in an oven at 140 °C for 4 h. The thickness of the printed Nafion-carbon ink layer or the backing layer was approximately 4 μm, as measured using calipers. The printed Pt_{50}–Ru_{50} catalyst layer on the GDL and the PEM were prepared using conventional screen-printing method and direct-printing method developed by Hsu and Wan [19] using a Pt_{50}–Ru_{50} as electrocatalyst, respectively. The hot pressing of the GDL electrode and the PEM-contained Pt_{50}–Ru_{50} layer form the anode electrode and the MEAs. The resulting anode catalyst loading was 1.63 mg cm^{-2}, of which the loading of the directly printed Pt_{50}–Ru_{50} layer on the PEM was only 0.40 mg cm^{-2}.

2.3. Preparation of cathode

The preparation of cathode catalyst ink was similar to that of Nafion-carbon ink. The only difference between the two inks was that a 40% Pt/C electrocatalyst was used in the former as opposed to Vulcan XC-72 carbon powder in the latter. The preparation of active cathode catalyst layers was similar to that of anode electrodes. The cathode catalyst layers of all the MEAs in this study include both catalyst layers on PEM and GDL. The obtained cathode catalyst loading is 2.26 mg cm^{-2}, of which the loading of the directly printed Pt layer on the PEM is 0.20 mg cm^{-2}.

2.4. Preparation of normal-MEA

The production process of the directly printed Pt_{50}–Ru_{50} or Pt layer on the PEM and the printed Pt_{50}–Ru_{50} or Pt layer on the GDL is similar to that of the anode and the cathode, as described in Sections 2.2 and 2.3. The hot pressing of the resulting anode and cathode formed the normal-MEA. The anode and cathode loadings of this MEA were similar to that of the MEA-I and MEA-II (see Table 1).

2.5. Preparation of membrane electrode assembly (MEA)

Nafion 117 (DuPont, Inc., USA) is used as a polymer electrolyte membrane in each case. Before it was applied, each membrane was first boiled in 3% hydrogen peroxide to remove any organic impurities, and then washed with water, followed by boiling in 1 M sulfuric acid to remove any metallic impurities and to fully convert the membrane to the H^+ form. Finally, the PEM was washed in deionized-water. The pre-treated PEM was then used in the production of a layer of nanometer-sized metal particles dispersed in PEM using the IR method. The PEM had a Pt_{50}–Ru_{50} layer that was directly printed on the anode side and a Pt layer on the cathode side. The PEM was then placed between the two GDL electrodes. Finally, the MEA was produced by applying a pressure of 9–10 MPa at 135 °C for 2 min.

2.6. Evaluation of electrode/MEA

The MEA was placed between two silicone gaskets, each 0.24 mm thick, and inserted between two graphite plates with serpentine grooves. It was then placed in a single cell test fixture (5 cm^2) supplied by Electrochem Inc., USA. A uniform torque of 80 kg_f cm was applied to the eight bolts that were used to assemble the DMFC. The fuel cell was connected to the test station (Fuel Cell Technologies, Inc., USA), which was equipped with a gas humidifier, a mass flow controller and a temperature controller with display. 2 M methanol and dry oxygen gas were fed into the cell at flow rates of 3 and 100 ml min^{-1}, respectively. The current–voltage (I–V)

characteristics and the rate of methanol crossover of the cell were measured at 80 °C in 2 M concentration of methanol.

2.7. Characterization of PEM-I and PEM-II

The X-ray diffraction (XRD) patterns for the deposited layers in PEM were measured via a PANalytical X-ray diffractometer X'Pert Pro using Cu Kα radiation source operating at 40 kV and 30 mA. The prepared composites were first examined with a field emission scanning electron microscope, FESEM (JEOL, JSM-6700F), then the distribution of the metal layers was analyzed by an energy-dispersive spectrometer, EDS (OXFORD INSTRUMENTS, INCAx-sight 7557). Compositions, thickness and distributions of the metal and alloy layers were later determined through an electron probe micro-analysis, EPMA (JEOL, JXA-8500F).

2.8. Evaluation of methanol crossover

The amount of crossed-over methanol at the cathode side was monitored by measuring the steady-state concentration of CO_2 in the cathode exhaust (after trapping water in an ice trap) using CO_2 sensor. The crossover rate of methanol was calculated from the production of CO_2. All CO_2 concentrations remain steady after 10 min into the test. The output current and voltage were measured when the concentration of CO_2 remains steady after 1 h.

3. Results and discussion

3.1. Microstructure and morphology of PEM-I and PEM-II

Fig. 2(A) shows a SEM image of the first deposited sub-layer of PEM-I. Apparently, the layer has a porous, coral-like, rather than a sphere-like surface microstructure. Grazing incident X-ray diffraction (GID) was used to obtain the XRD pattern at an X-ray incidence angle of 1° to verify the phases of the cluster particle layer. Fig. 3(A) presents XRD pattern of the first deposited sub-layer in PEM-I. It includes characteristic peaks of the Pt element at 39.5°, 46.1° and 67.8°. These are the peaks associated with the Pt (1 1 1), Pt (2 0 0) and Pt (2 2 0) faces, indicating the first deposited sub-layer in PEM-I is a layer of pure Pt.

The EPMA result from the cross-sectional view of the first deposited sub-layer is shown in Fig. 4. The sulfur elemental dis-

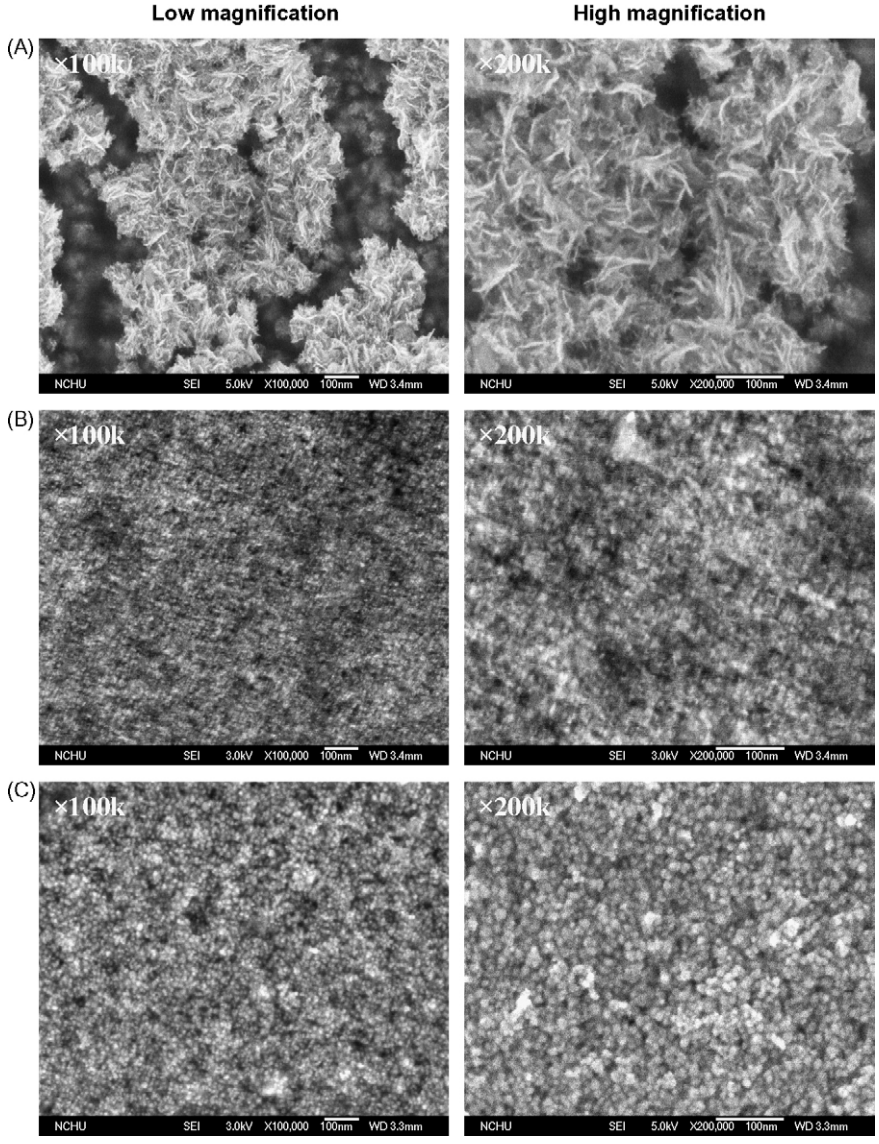

Fig. 2. SEM images (100k× and 200k×) of (A) first Pt sub-layer in PEM-I; (B) second Pt_{37}–Ru_{63} sub-layer in PEM-I; (C) first Pt_{20}–Ru_{80} sub-layer in PEM-II.

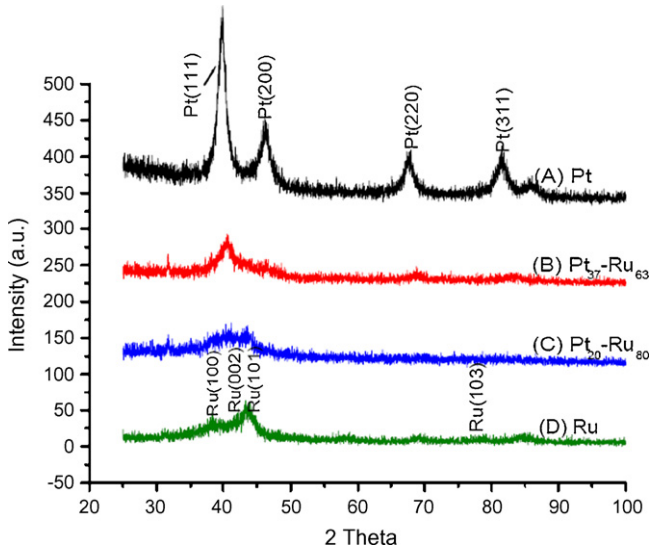

Fig. 3. X-ray diffraction patterns from (A) first deposited Pt sub-layer in PEM-I; (B) second deposited Pt_{37}–Ru_{63} sub-layer in PEM-I; (C) first deposited Pt_{20}–Ru_{80} sub-layer in PEM-II; (D) deposited pure Ru in PEM surface using IR method.

tribution profile represents the distribution of Nafion conducting proton as well as the existence of PEM. Evidently, only the Pt element exists in the PEM surface. The onset peak position in the sulfur elemental distribution profile precedes that of Pt elemental distribution profile by 0.5 μm while the thickness of Pt layer is 2.0 μm, as determined by measuring the position of the peaks of Pt and S elements (the width of the half peak height is defined as the thickness). This result suggests that the first deposited sub-layer of Pt locates at a distance of 0.5 μm from the PEM surface with a thickness of 2.0 μm.

Fig. 2(B) depicts the surface microstructure of the second deposited sub-layer of PEM-I. The observed microstructure is clearly different from the first sub-layer and is in the form of clusters with sizes of approximately 10 nm. The XRD pattern of the second sub-layer is shown in Fig. 3(B). Fig. 3(D) shows the XRD pattern of the pure Ru that was deposited via the IR method. Clearly, the second deposited layer has the characteristic peaks of Pt and Ru. The characteristic peak of the Pt element is strong and sharp at 39.6°, and is associated with the Pt (1 1 1) face (as shown in Fig. 3(A)). In contrast, no peak is observed at the corresponding peak position for pure Ru. Accordingly, the Pt (1 1 1) face peak is selected as the reference peak to confirm the presence of the alloy phase by comparing the lattice constants of pure Pt and the obtained Pt–Ru. Bragg's equation yields a lattice constant of 3.920 Å for pure Pt and 3.804 Å for Pt–Ru, respectively. The lattice constant of Pt–Ru is clearly smaller than that of pure Pt, suggesting that the second deposited sub-layer of PEM-I is a Pt–Ru alloy [17]. The intensity of the peak at 40.9° from the deposited Pt–Ru is lower than that of pure Pt, indicating that the elemental Pt content in the alloy is low. The substrate effect of the GID method prevents the determination of the composition of the thin film from the lattice parameter derived from XRD. EPMA, on the other hand, can accurately measure the atomic ratio of the thin film, and is applied to determine the composition of the thin film. The EPMA result (an average over 25 sampling points) demonstrates that the atomic ratio of Pt:Ru is 37:63.

Fig. 5 presents the EPMA results from the cross-sectional view of the PEM-I with two deposited sub-layers. The onset peak positions in the Pt and Ru elemental distribution profiles are the same as that of the sulfur elemental distribution profile, indicating the second layer is deposited on the PEM surface. Both the Pt and Ru elemental distribution profiles show only one peak, indicating that no layer boundary exist between the first and the second sub-layer. Most of the Ru element is distributed near the PEM surface with a thickness of 1.5 μm, while the Pt element is concentrated at the PEM surface with the thickness of 2.5 μm. Therefore, the second alloy sub-layer is deposited on the PEM surface with the thickness of 1.5 μm and the first deposited Pt layer is distributed at a distance of 1.5 μm from the PEM surface with the thickness of 1.0 μm.

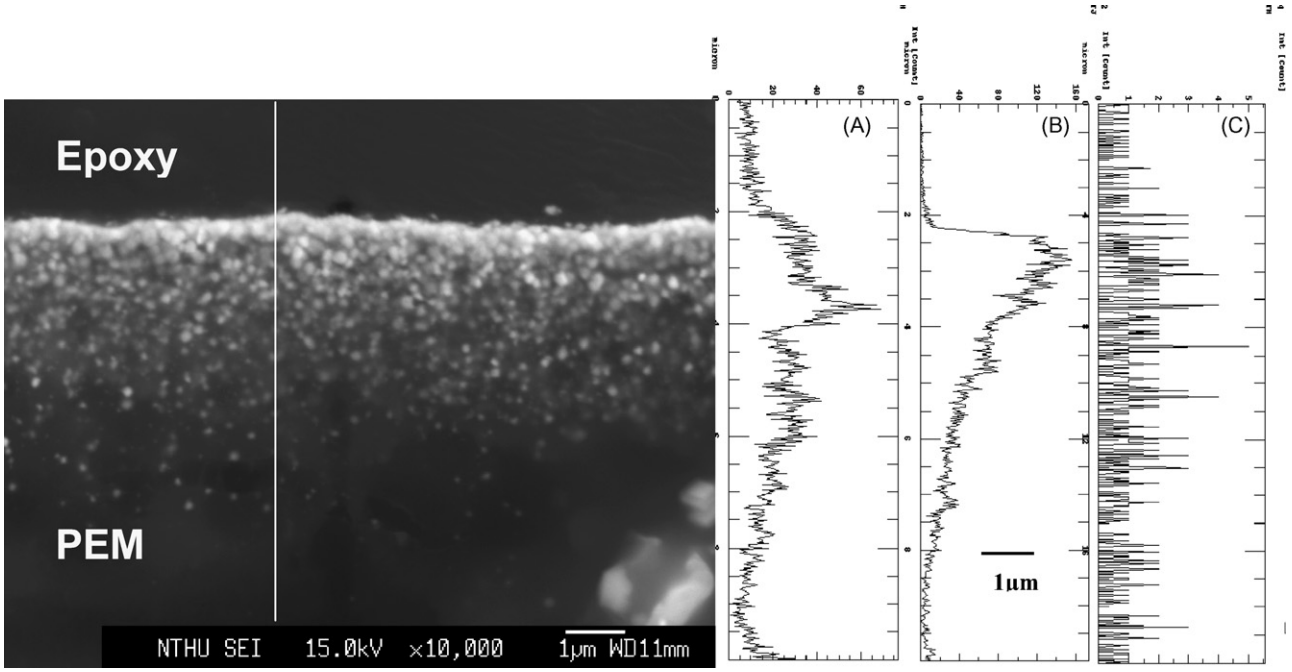

Fig. 4. Cross-sectional view EPMA image (10k×) of PEM-I with first Pt sub-layer (white line represents sampling line): (A) elemental S distribution profile; (B) elemental Pt distribution profile; (C) elemental Ru distribution profile.

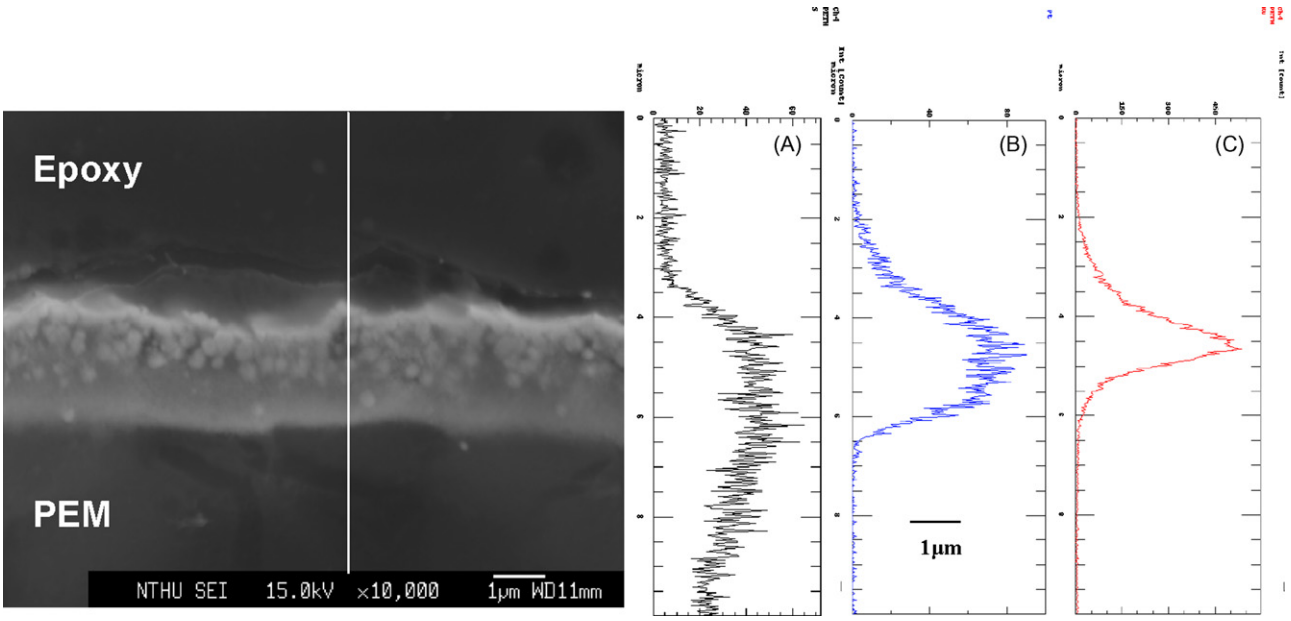

Fig. 5. Cross-sectional view EPMA image (10k×) of PEM-I with two sub-layers (white line represents sampling line): (A) elemental S distribution profile; (B) elemental Pt distribution profile; (C) elemental Ru distribution profile.

Consequently, the total thickness is approximately 2.5 μm. Notice, this result is not consistent with the EPMA result of PEM-I with only first deposited Pt sub-layer because the second alloy sub-layer is not solely deposited in the region that spans 0.5 μm from the PEM surface. This result can be attributed to the impregnation process in the IR method, in which the precursors of Pt and Ru may impregnated through the metal Pt layer during the second treatment of impregnation in the presence of methanol. The PEM expands (swelling) in the presence of methanol. As a result, the reductant $NaBH_4$ can pass through the metal Pt layer and deposits a second sub-layer further into the PEM with a layer thickness of 1.5 μm. Due to the nature of concentration distribution of precursors in the PEM surface, when ion-exchange (proton) occurs through diffusion mass transfer, no layer boundary exists between the first and second deposited sub-layer.

The structure of PEM-II is similar to that of PEM-I. The only difference between them is in the first deposited sub-layer in PEM, which is a layer of Pt_{20}–Ru_{80} in PEM-II as opposed to a layer of pure Pt in PEM-I. Fig. 2(C) shows a SEM image of the first deposited sub-layer of PEM-II. It clearly shows a sphere-like microstructure that is different from that presented in Fig. 2(B). The particles form clusters with sizes ranging from 10 to 13 nm. Fig. 3(C) presents the XRD pattern obtained at an X-ray incidence angle of 1° from the first deposited layer of PEM-II. As in PEM-I, the Pt (1 1 1) face peak is selected as the reference peak to confirm the presence of the alloy phase. Bragg's equation yields a lattice constant of 3.735 Å for this layer. The lattice constant is clearly smaller than that of the pure Pt, indicating the presence of an alloy phase in the first sub-layer of PEM-II. The intensity of the Pt (1 1 1) face peak is relatively lower than that of the peak exhibited in Fig. 3(B), suggesting that the elemental Pt content in the Pt–Ru alloy is lower than 37%. The XRD and EPMA results (an average over 25 sampling points) verify that the nano-clusters are of Pt–Ru alloy with an atomic ratio of 20:80. The EPMA result from the cross-sectional view of the PEM-II with only first deposited sub-layer was adopted to verify the existence of a deeper layer. Fig. 6 shows that the onset peak position in the sulfur elemental distribution profile precedes that of the Pt and Ru elemental distribution profiles by about 1.0 μm. The thickness of Pt and Ru elemental distribution is approximately 2.0 μm, indicating the deeper layer is located at a distance of 1.0 μm from the PEM surface with a thickness of 2.0 μm.

The second deposited sub-layer of PEM-II is the same as that of PEM-I, i.e., Pt_{37}–Ru_{63} layer. It has a similar surface microstructure and XRD pattern to that of the second deposited layer of PEM-I, as shown in Figs. 2(B) and 3(B), respectively. Fig. 7 plots an EPMA cross-sectional view of PEM-II with two deposited sub-layers. The onset peak position in Pt and Ru elemental distribution profiles are the same as that of the sulfur elemental distribution profile, indicating that the second deposited layer is located at the PEM surface. There is only one peak exhibited in the Pt and Ru elemental distribution profiles, indicating the second deposited layer of Pt_{37}–Ru_{63} and the first deposited layer of Pt_{20}–Ru_{80} are completely mixed. The total thickness is approximately 3.0 μm, which is similar to that of PEM-I. Consequently, PEM-II has a layer of nanometer-sized Pt_{37}–Ru_{63}/Pt_{20}–Ru_{80} catalyst particles dispersed in PEM surface with a layer thickness of 3.0 μm. Most of the Pt_{37}–Ru_{63} catalyst is distributed close to the direct-printed catalyst layer, while the Pt_{20}–Ru_{80} catalyst is rich in the deeper layer.

3.2. Polarization curves and rate of methanol crossover

Fig. 8 shows the variation of crossover rate as a function of the current density drawn from the DMFCs at cell temperature of 80 °C with dry oxygen fed to the cathode under ambient pressure. The $\boldsymbol{j}(CH_3OH)$ represents the equivalent current density for the oxidation of crossed-over methanol. The variation in cell potential, simultaneously measured, is also shown in Fig. 9. The value of $\boldsymbol{j}(CH_3OH)$ decreases with increasing output current density (see Fig. 8). This is because the methanol concentration at the anode/membrane interface decreases with increasing faradaic consumption of methanol. Figs. 8 and 9 clearly show that the $\boldsymbol{j}(CH_3OH)$ is reduced and the voltage is enhanced in all polarization regions for the MEA comprising of dispersed Pt_{37}–Ru_{63}/Pt or Pt_{37}–Ru_{63}/Pt_{20}–Ru_{80} particles in PEM. For example, at T_{cell} = 80 °C and at 50 mA cm^{-2} with 2 M concentration of methanol, the $\boldsymbol{j}(CH_3OH)$ for MEA-I and MEA-II are about 78% and 67% of that in normal-MEA, respectively, and the potential gains are approximately 33 and 53 mV, respectively. MEA consisting of a layer of

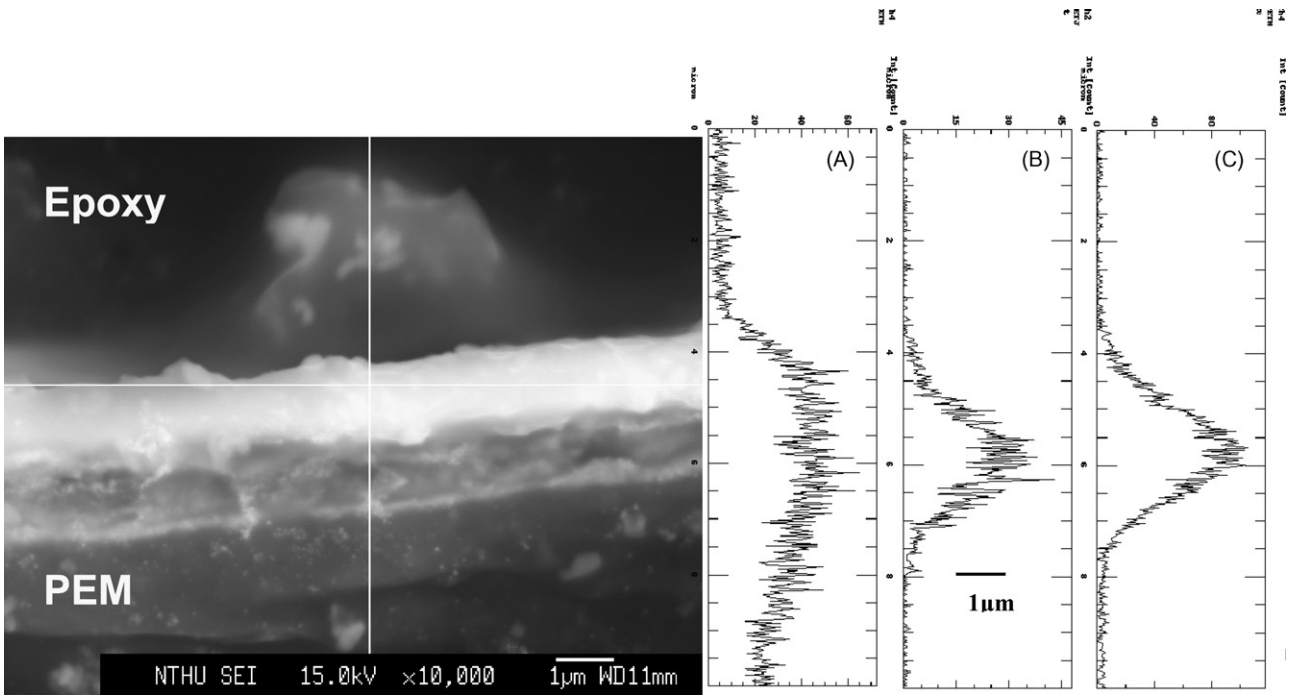

Fig. 6. Cross-sectional view EPMA image (10k×) of PEM-II with first Pt_{20}–Ru_{80} sub-layer (white line represents sampling line): (A) elemental S distribution profile; (B) elemental Pt distribution profile; (C) elemental Ru distribution profile.

Pt_{37}–Ru_{63}/Pt_{20}–Ru_{80} particles deposited in PEM surface possesses the best cell performance and suppression of methanol crossover among the MEAs mentioned in this paper.

Comparing the values between the decreased crossed-over current density and the increased output current density for MEA-I and MEA-II, it shows that the increase of the output current density is greater than the decrease of the crossed-over current density. For example, at an output voltage of 0.30 V, the increase of output current densities for MEA-I and MEA-II are approximately 14.3 and 22.9 mA cm^{-2} more than that of the normal-MEA, while the decrease of the crossed-over current densities are 11.3 and 16.5 mA cm^{-2}, respectively. Furthermore, the amount of CO_2 at the anode side is higher for both MEA-I and MEA-II as compared to normal-MEA. The most probable mechanism through which explains the above results is a layer of Pt_{37}–Ru_{63}/Pt or Pt_{37}–Ru_{63}/Pt_{20}–Ru_{80} particles dispersed in PEM

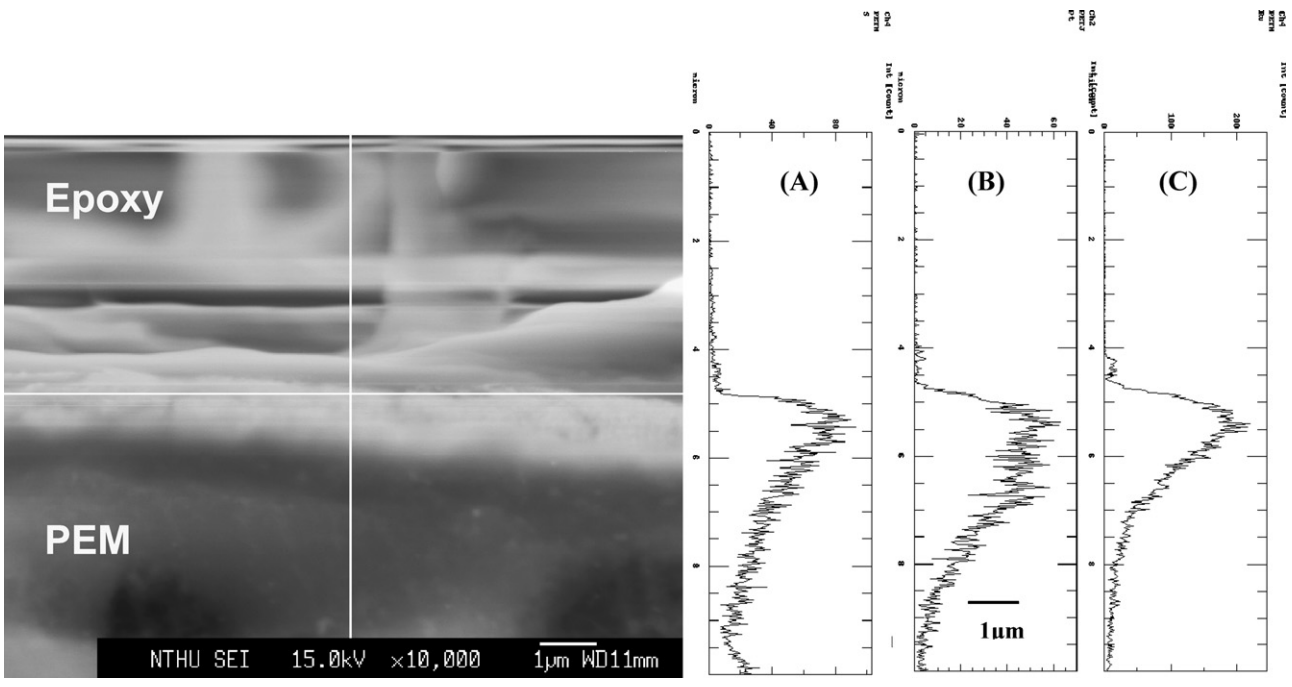

Fig. 7. Cross-sectional view EPMA image (10k×) of PEM-II with two sub-layers (white line represents sampling line): (A) elemental S distribution profile; (B) elemental Pt distribution profile; (C) elemental Ru distribution profile.

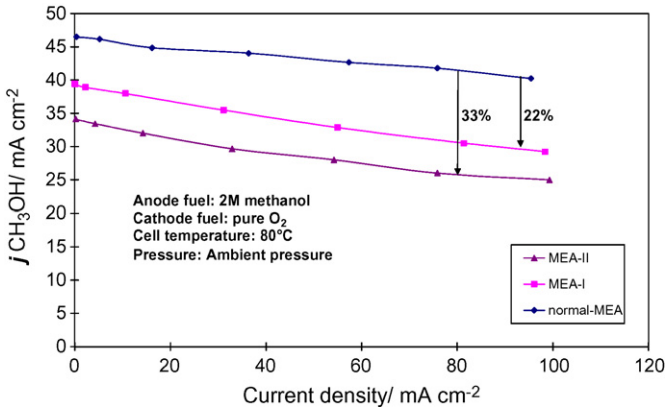

Fig. 8. Plots of the equivalent current density for the oxidation of crossed-over methanol, $j(CH_3OH)$, in normal-MEA, MEA-I and MEA-II as a function of the output current density in DMFCs operated at T_{cell} = 80 °C under ambient pressure. The feed rates of 2 M methanol and dry oxygen gas were 3 and 100 ml min^{-1}, respectively.

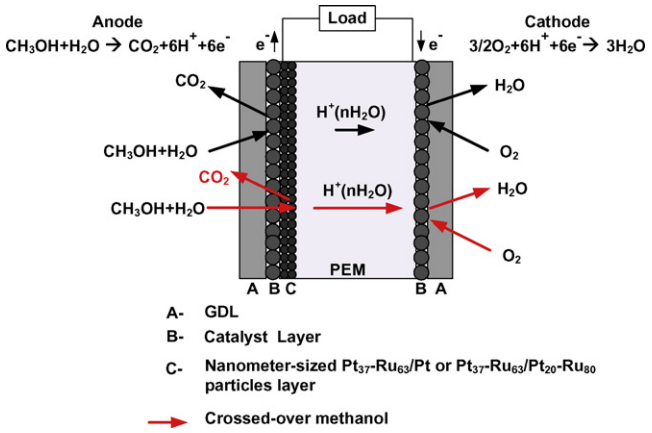

Fig. 10. Diagram of the proposed mechanism for suppression of methanol crossover.

reduces the deleterious effects of crossover by catalytic reaction of the crossed-over methanol with dispersed catalyst particles in PEM. The electrons generated from the oxidation of crossed-over methanol are conducted to the external circuit through the direct-printed catalyst layer on PEM, while the protons are transferred to cathode through the PEM. The resulted CO_2 diffuses to the anode and thus increases the CO_2 concentration at the anode. In addition, a layer of nanometer-sized Pt_{37}–Ru_{63}/Pt or Pt_{37}–Ru_{63}/Pt_{20}–Ru_{80} particles dispersed in PEM anode side also serves as an electrode to oxidize the anode methanol fuel at the interface between the middle layer and the second sub-layer in the inner layer. The combination of these two effects improves cell performance and utilization efficiency of methanol fuel as well as suppresses methanol crossover. Therefore, a layer of nanometer-sized Pt_{37}–Ru_{63}/Pt or Pt_{37}–Ru_{63}/Pt_{20}–Ru_{80} particles dispersed in PEM surface acts as the reactive methanol "filter". The proposed mechanism for the suppression of methanol crossover and the enhancement of cell performance are presented in Fig. 10.

The performance and suppression of methanol crossover of MEA-II outperforms that of MEA-I at 80 °C in 2 M concentrations of methanol. As mentioned above, the only difference between MEA-I and MEA-II is in the PEM structure, i.e., a layer of pure Pt in the first sub-layer of PEM-I as opposed to a layer of Pt_{20}–Ru_{80} alloy in the first sub-layer of PEM-II. Consequently, the presence of Ru elements in the first sub-layer substantially improves the cell performance and the suppression of methanol crossover due

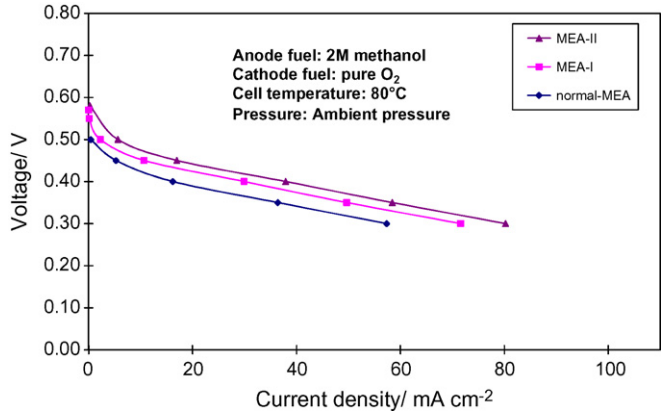

Fig. 9. Polarization curves for various MEAs fed with 2 M methanol fuel at 80 °C (cell temperature) under ambient pressure.

to the better CO tolerance of Pt–Ru alloy than that of the pure Pt. This result further confirms the proposed mechanism for the suppression of methanol crossover and improvement of performance using a layer of nanometer-sized catalyst particle deposited in PEM surface.

Note that there are significant differences between the structures of PEM in this study and the structure of PEM developed by Uchida et al. [18]. As mentioned above, the PEMs reported in this paper have a layer of nanometer-sized Pt_{37}–Ru_{63}/Pt or Pt_{37}–Ru_{63}/Pt_{20}–Ru_{80} particles deposited at the surface of PEM anode side. In contrast, the Uchida's PEM has nanometer-sized Pt particles highly dispersed into the PEM without forming a layer and concentrating at the surface of the PEM. Furthermore, the nanometer-sized catalyst in our PEM is Pt_{37}–Ru_{63}/Pt or Pt_{37}–Ru_{63}/Pt_{20}–Ru_{80} particles as opposed to a highly dispersed nanometer-sized Pt in Uchida's PEM. Finally, the mechanism that suppresses the methanol crossover is vastly different between the two PEMs. For our PEM, the crossed-over methanol is oxidized to produce electrons, protons and CO_2 as it crosses through a layer of nanometer-sized Pt_{37}–Ru_{63}/Pt or Pt_{37}–Ru_{63}/Pt_{20}–Ru_{80} particles deposited at the surface of PEM anode side. The nanometer-sized Pt_{37}–Ru_{63}/Pt or Pt_{37}–Ru_{63}/Pt_{20}–Ru_{80} particles form a conducting layer through which the resulted electrons can flow to the external circuit and transfer to the cathode side. As a result, it suppresses the methanol crossover and improves the performance. In contrast, the crossed-over methanol in Uchida's PEM is reacted with oxygen diffused from cathode to yield CO_2 and water as methanol crosses through a nanometer-sized Pt particle dispersed into the PEM. This mechanism significantly improves the performance of both electrodes, particularly the cathode. This is due to the reduced amount of methanol arriving at the cathode, as compared to that occurring in the PEM without nanometer-sized Pt particles.

Table 2 compares the suppression of methanol crossover and performance of DMFC between our PEM and Uchida's PEM. Our PEM with nanometer-sized catalyst loading of 0.52 mg cm^{-2} suppresses methanol crossover up to 33% and improves the voltage output up to 18%. Meanwhile, Uchida's PEM with loading of 0.10 mg cm^{-2} suppresses methanol crossover up to 30% and improves the voltage output up to only 7%. The comparison clearly shows that the proposed structure of PEM in this study outperforms the structure of PEM developed by Uchida et al. in terms of electrochemical performance and suppression of methanol crossover. Note that the anode catalyst is pure Pt (not Pt_{50}–Ru_{50}) for the MEA developed by Uchida et al. The loading of nanometer-sized catalyst deposited in PEM, anode loading and cathode loading for our PEM are different from that of the Uchida's

Table 2
Comparison of the electrochemical performance and suppression of methanol crossover between the MEAs in this paper and the MEAs proposed by Uchida et al. [18].

Sample code	Loading of inner layer		Total anode loading ($mg\ Pt_{50}–Ru_{50}\ cm^{-2}$)	Total cathode loading ($mg\ Pt\ cm^{-2}$)	Degree of suppression of methanol crossover[a] (%)	Potential gain (%)
	First sub-layer	Second sub-layer				
MEA-I	$0.25\ mg\ Pt\ cm^{-2}$	$0.27\ mg\ Pt_{37}–Ru_{63}\ cm^{-2}$	1.63	2.26	22	12
MEA-II	$0.25\ mg\ Pt_{20}–Ru_{80}\ cm^{-2}$	$0.27\ mg\ Pt_{37}–Ru_{63}\ cm^{-2}$	1.63	2.26	33	18
MEA-Pt[b]	$0.10\ mg\ Pt\ cm^{-2}$		$2.00\ mg\ Pt\ cm^{-2}$	2.00	30[c]	7
MEA-Pt–Ru[b]	$0.10\ mg\ Pt\ cm^{-2}$		2.60	2.40	–	–

[a] The results were obtained at $T_{cell} = 80\ ^\circ C$ and at $50\ mA\ cm^{-2}$ with 2 M methanol.
[b] MEAs in Ref. [18].
[c] This result was obtained at $T_{cell} = 80\ ^\circ C$ and at $100\ mA\ cm^{-2}$ with 1 M methanol.

PEM. Methanol concentration used is also different between the two.

4. Conclusions

A layer of nanometer-sized $Pt_{37}–Ru_{63}$/Pt or $Pt_{37}–Ru_{63}/Pt_{20}–Ru_{80}$ catalyst particles deposited on the PEM anode side with a total thickness of 2.5 μm or 3.0 μm are successfully prepared using the IR method according to the designed conditions and procedures. There is no layer boundary exists between first and second deposited sub-layers. The MEA-I and MEA-II, comprising a layer of nanometer-sized $Pt_{37}–Ru_{63}$/Pt and $Pt_{37}–Ru_{63}/Pt_{20}–Ru_{80}$ catalyst particles dispersed in PEM, respectively, can markedly suppress methanol crossover and increase cell performance. This is especially true for MEA-II since it can better suppress methanol crossover, i.e., approximately 33%, with 18% improvement in performance. This is because the crossed-over methanol is simultaneously oxidized by a layer of $Pt_{37}–Ru_{63}$/Pt or $Pt_{37}–Ru_{63}/Pt_{20}–Ru_{80}$ nano-particles dispersed in PEM anode side surface to form CO_2, electrons and protons. The resulted electrons and protons transfer through the direct-printed catalyst layer via external circuit and PEM to cathode, respectively. In addition, a layer of nanometer-sized $Pt_{37}–Ru_{63}$/Pt or $Pt_{37}–Ru_{63}/Pt_{20}–Ru_{80}$ particles deposited on PEM surface serves as the anode electrode to oxidize the methanol fuel. As a result, it "filters" out the crossed-over methanol and improves the cell performance as well as the utilization efficiency of methanol fuel. Due to the better CO tolerance of Pt–Ru alloy, incorporating Pt–Ru alloy in both sub-layers in the PEM surface can increase the suppression of methanol crossover and the performance.

Acknowledgement

The authors would like to thank the National Science Council of the Republic of China, Taiwan, for financially supporting this research under Contract No. NSC 95-2221-E-451-007.

References

[1] A. Heinzel, V.M. Barragan, J. Power Sources 84 (1999) 70–74.
[2] G.T. Burstein, C.J. Barnett, A.R. Kucernak, K.R. Williams, Catal. Today 38 (1997) 425–437.
[3] M. Hogarth, P. Christensen, A. Hamnett, A. Shukla, J. Power Sources 69 (1997) 113–124.
[4] T. Frelink, W. Visscher, J.A.R. van Veen, Surf. Sci. 335 (1995) 353–360.
[5] B.R. Rauhe, J.F.R. Mclarnon, E.J. Cairns, J. Electrochem. Soc. 142 (1995) 1073–1084.
[6] T. Frelink, W. Visscher, A.P. Cox, J.A.R. van Veen, Electrochim. Acta 40 (1995) 1537–1543.
[7] X. Ren, T.E. Springer, S. Gottesfeld, J. Electrochem. Soc. 147 (2000) 92–98.
[8] J.S. Wainright, J.-T. Wang, D. Weng, R.F. Savinell, M. Litt, J. Electrochem. Soc. 142 (1995) L121–L123.
[9] M. Weng, J.S. Wainright, U. Landau, R.F. Savinell, J. Electrochem. Soc. 143 (1996) 1260–1263.
[10] J.-T. Wang, S. Wasmus, R.F. Savinell, J. Electrochem. Soc. 143 (1996) 1233–1239.
[11] S. Wasmus, J.-T. Wang, R.F. Savinell, J. Electrochem. Soc. 142 (1995) 3825–3833.
[12] V. Tricoly, J. Electrochem. Soc. 145 (1998) 3798–3801.
[13] C. Pu, W. Huang, K.L. Ley, E.S. Smotkin, J. Electrochem. Soc. 142 (1995) L119–L120.
[14] H. Takenaka, Kokai Tokkyo Koho, Japan Patent No. 57-134586 (1982).
[15] P.S. Fedkiw, W.-H. Her, J. Electrochem. Soc. 136 (1989) 899–900.
[16] R. Liu, W.-H. Her, P.S. Fedkiw, J. Electrochem. Soc. 139 (1992) 15–23.
[17] N. Fujiwara, K. Yasuda, T. Ioroi, Z. Siroma, Y. Miyazaki, Electrochim. Acta 47 (2002) 4079–4084.
[18] H. Uchida, Y. Mizuno, M. Watanabe, J. Electrochem. Soc. 149 (2002) A682–A687.
[19] C.H. Hsu, C.C. Wan, J. Power Sources 115 (2003) 268–273.